Journal of Magnetism and Magnetic Materials 582 (2023) 171030

Contents lists available at ScienceDirect

Journal of Magnetism and Magnetic Materials

journal homepage: www.elsevier.com/locate/jmmm

Research article

Anomalies in the magnetic properties of bismuth-substituted diluted yttrium iron garnet

S.S. Aplesnin [a,b,*], F.V. Zelenov [b], S.V. Semenov [a,c], O.A. Bayukov [a]

[a] Kirensky Institute of Physics, Federal Research Center KSC SB RAS, Akademgorodok, 50, Krasnoyarsk 660036, Russia
[b] Reshetnev Siberian State University of Science and Technology, Krasnoyarsky Rabochy Av., 31, Krasnoyarsk 660014, Krasnoyarsk, Russia
[c] Siberian Federal University, Svobodny pr. 79, Krasnoyarsk 660041, Russia

ARTICLE INFO

Keywords:
Magnetic properties
Compensation temperature
Mossbauer spectroscopy

ABSTRACT

The magnetic properties and Mössbauer spectra of the $Y_{1.8}Bi_{1.2}Fe_{3.5}Ga_{1.5}O_{12}$ compound were investigated. A linear temperature dependence of the saturation magnetization, hysteresis, and stability of the coercive field in the magnetically ordered state were found. Using the Mössbauer measurements, the distribution of iron ions over octahedral and tetrahedral sites and the concentration of paramagnetic iron ions were determined. Two critical temperatures – the sublattice magnetization compensation temperature and the ferrimagnet–paramagnet transition temperature – were established. The disappear of the phonon mode in the vicinity of the magnetic transition was observed. The experimental data have been interpreted in terms of the spin–lattice interaction model.

1. Introduction

Yttrium iron garnet (YIG) is interesting for both fundamental research and application. In YIG, magnons propagate to distances that exceed the distances of propagation of spin-polarized electrons by orders of magnitude [1]; the use of optical magnons [2] can accelerate data processing and makes YIG promising for magnon spintronics [3]. Substitution of bismuth for yttrium intensifies the Faraday effect [4] and expands the range of magneto-optical applications [5].

According to the theoretical calculations in the molecular field approximation [6,7], gallium-substituted YIGs can have the substitution concentration-dependent temperature of the sublattice magnetic moment compensation, which increases from 0 to 400 K. In the vicinity of the compensation temperature, the magnetization dynamics can be controlled on a femtosecond scale, which opens up prospects for the development of integrated opto-spintronic devices [8–11]. In the experiments, the compensation temperature was not observed because of the difference between the distributions of gallium cations over tetrahedral (*a*) and octahedral (*d*) sites, which depend on a sample fabrication technique used. The distributions of diamagnetic Ga ions over octahedral and tetrahedral sites in the polycrystalline and single-crystal samples are different [6,7]. In $Y_3[Fe_{2-x}Ga_x](Fe_{3-y}Ga_y)O_{12}$ ($x + y = 1.5$), the Ga concentration in tetrahedral sites is $y = 1.3$ for polycrystals and $y = 1.36$ for single crystals. The Curie temperature is $T_C = 348$ K and the saturation magnetization at $T = 4.2$ K at a gallium concentration of $\times + y = 1.5$ decreases by a factor of 5. The magnetization is described by the power dependence $M(T) = M_0(1 - T/T_C)^{\beta}$ ($\beta = 0.6$) and the magnetic anisotropy field is $H_a = H_0(1 - T/T_C)^{\alpha}$ ($\alpha > 1$). The frequency of the Raman mode of the Fe–O bond vibrations in $YFe_{5-x}Ga_xO_{12}$ increases from 498 cm^{-1} at $x = 0$ to 505 cm^{-1} at x = 1 [12]. The bond length decreases from Fe_d–O = 0.2036 nm at x = 0 to 0.2016 nm at x = 1 in the octahedron and increases from Fe_a–O = 0.1846 nm at x = 0 to 0.1855 nm at x = 1 in the tetrahedron. The saturation magnetization M_S decreases linearly from 28.2 emu/g at x = 0 to 4.98 emu/g at x = 1.0, possibly, due to the formation of a noncollinear spin structure [12]. In the Mössbauer spectra, five nonequivalent positions of Fe^{3+} ions in $YFe_{5-x}Ga_xO_{12}$ at x = 1 were found. Three of them correspond to Fe^{3+} ions in octahedral sites with a weight of 0.39 and two correspond to Fe^{3+} ions in tetrahedral sites with a weight of 0.61. The appearance of new components is attributed to the formation of several clusters of Ga^{3+} ions that are the nearest neighbors of Fe^{3+} ions.

Substitution of bismuth for yttrium induces the magnetoelectric interaction. The magnetoelectric effect, which is explained by the spin–orbit coupling [13–16], was observed at domain walls [17–19] and in thin films. The modes in the range of 700–500 cm^{-1} shift to the low-temperature region and the modes in the range of 500–400 cm^{-1} assigned to the octahedron undergo a blue shift upon substitution of bismuth for yttrium [20–21]. The infra-red (IR) spectra of $Y_2Bi_1Fe_3O_{12}$

* Corresponding author at: Kirensky Institute of Physics, Federal Research Center KSC SB RAS, Akademgorodok, 50, Krasnoyarsk 660036, Russia.
E-mail addresses: apl@iph.krasn.ru, apl@iph.krasn.ru (S.S. Aplesnin).

https://doi.org/10.1016/j.jmmm.2023.171030
Received 31 March 2023; Received in revised form 22 June 2023; Accepted 9 July 2023
Available online 13 July 2023

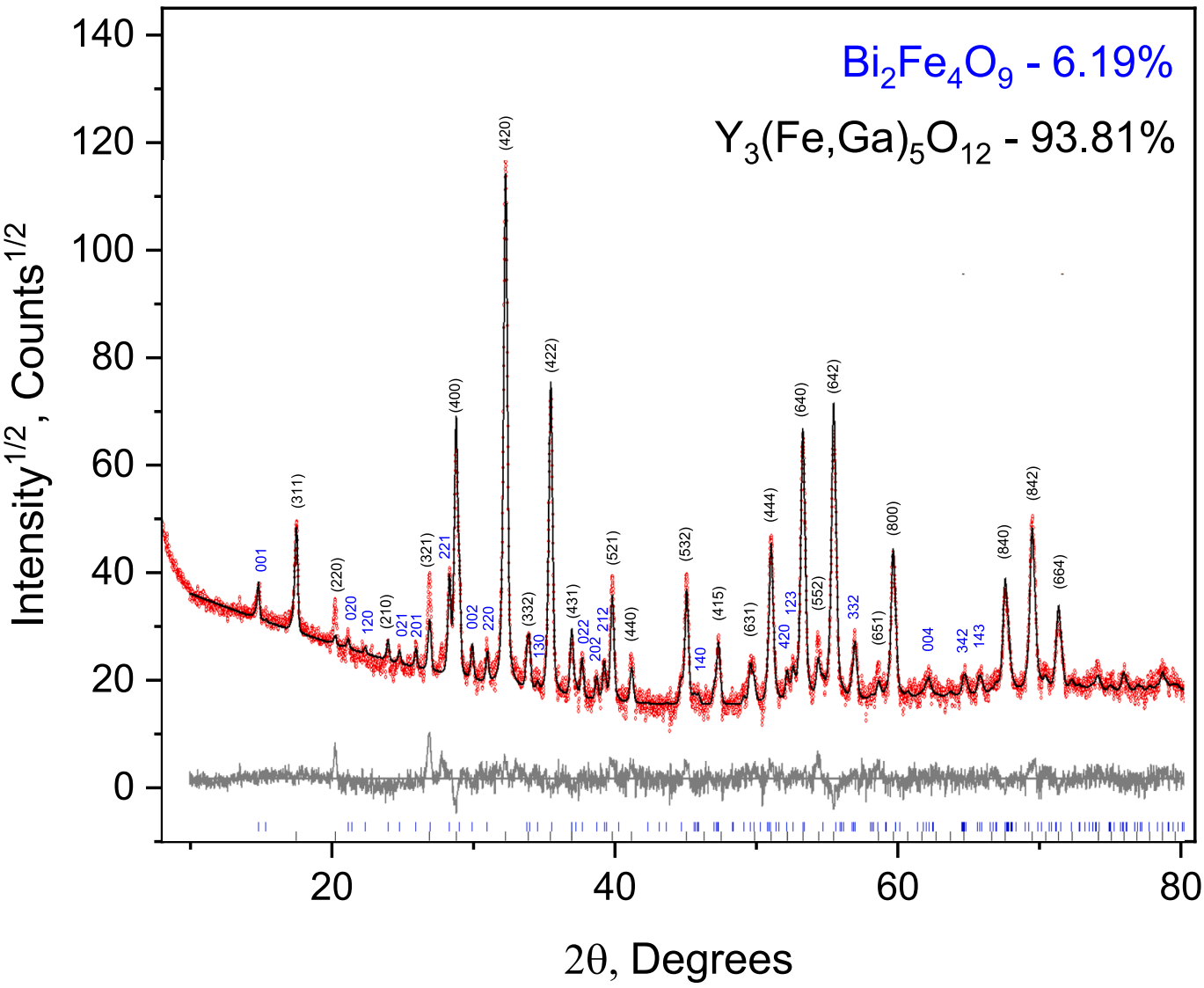

Fig.1. X-ray diffraction pattern of the $Y_{1.8}Bi_{1.2}Fe_{3.5}Ga_{1.5}O_{12}$ and $Bi_2Fe_4O_9$ at room temperature.

contain an additional absorption maximum at a frequency of 850 cm^{-1}, which is not observed for YIG. At $T = 10$ K, the magnetic moment per formula unit decreases from 4.55 μ_B at x = 0 to 3.96 μ_B at x = 1. The coercivity of $Y_2Bi_1Fe_3O_{12}$ increases by a factor of two from $H_C = 35$ Oe ($T = 10$ K) to $H_C = 65$ Oe ($T = 300$ K) upon heating [20]. Bismuth ions located in dodecahedrons affect not only the indirect Fe–O–Fe exchange couplings, but also the value of the magnetic moment due to addition of the excited T_{2g} states. Possibly, shortening of the Fe–O bond lengths induces the transition from the high-spin (HS, S = 5/2) to low-spin (LS, S = 1/2) state under chemical pressure.

In the $Ba_3NbFe_3Si_2O_{14}$ multiferroic with a langasite structure, a spin crossover was found at a pressure of 50 GPa, when Fe^{3+} ions in oxygen octahedra pass from the high-spin (HS, S = 5/2) to low-spin (LS, S = 1/2) state. The temperature of the magnetic ordering of the LS sublattice is 22 K and the magnetic correlations between the HS and LS sublattices are observed [22]. The ultrahigh quadrupole splitting parameter (QS = 1.7 mm/s) determined from the Mössbauer spectra at $P > 50$ GPa characterizes the LS state of Fe^{3+} ions with a hyperfine field of H_{sf} = (8–9) T. Spin transitions occur on the iron ions surrounded by six ligands of the organic complexes [23]. The organic compounds with a crystal structure, e.g., $[Fe(NH_2trz)_3](NO_3)_2$, which undergoes the LS–HS spin transition around room temperature, were synthesized [24].

The ionic radius of the gallium ion is less than that of the trivalent iron ion. Therefore, gallium ions preferentially occupy tetrahedral positions. With an ideal substitution of iron ions by gallium, the concentration of iron ions in tetrahedral positions will decrease and, according to theoretical calculations, in the molecular field approximation, the sublattice magnetizations are compensated (compared) in the room temperature range in the concentration range X_{Ga} = 1.2–1.5. The substitution of yttrium by bismuth with a lone electron pair causes a redistribution of the electron density between the Bi-O-Fe ions, which leads to the modulation of the exchange and spin–orbit interaction. The magnetic anisotropy sharp increases. The strong electron–phonon interaction on the Bi-O bond creates the prerequisites for the existence of a non-Heisenberg exchange interaction between spins.

The aim of this study was to explore the effect of diamagnetic dilution on the formation of a compensation point in the $Y_{1.8}Bi_{1.2}Fe_{3.5}Ga_{1.5}O_{12}$ compound as a result of the selective distribution of gallium ions over tetrahedral and octahedral sites. The bismuth substitution increases the spin–orbit coupling, reduces the spin at the site, and enhances the spin–lattice coupling, which can lead to the formation of a non-Heisenberg exchange interaction between spins and anomalous temperature behavior of the magnetization.

Table 1
Structural parameters of the $Y_{1.8}Bi_{1.2}Fe_{3.5}Ga_{1.5}O_{12}$ and $Bi_2Fe_4O_9$.

	$Y_{1.8}Bi_{1.2}Fe_{3.5}Ga_{1.5}O_{12}$	$Bi_2Fe_4O_9$
Sp. gr.	Ia-3d	*Pbam*
a, Å	12.42953(38)	7.96795 (2)
b, Å	12.42966(38)	8.45160 (3)
c, Å	12.42966(38)	6.01100 (2)
β, °	90	90 (2)
V, Å^3	1920.28(18)	404.792661 (3)
2θ range,°	8–90	
R_{wp}, %	9.06	
R_p, %	7.01	
R_B, %	3.01	
χ^2	1.61	

2. Materials and methods

Polycrystalline $Y_{1.8}Bi_{1.2}Fe_{3.5}Ga_{1.5}O_{12}$ samples were synthesized by burning a gel with polyvinyl alcohol. The starting substances were yttrium and bismuth oxides, metallic gallium, and carbonyl iron (all of high purity), stoichiometric amounts of which were dissolved in dilute nitric acid. After dissolution, excess nitric acid was evaporated and citric acid was added to the nitrate solution as a complexing agent and ethylene glycol as a gelling component. The reaction mixture was evaporated (~100 °C) with continuous stirring to a gel state in which the primary components were homogenized at the molecular level. As the temperature increased, there was slow combustion of the gel to form a homogeneous mixture of chemically active oxides in the form of a finely dispersed powder. After cooling the powders were grinded, pressed into tablets and annealed at temperatures of 1000 °C with holding times 12 h [25].

The powder diffraction data on the $Y_{1.8}Bi_{1.2}Fe_{3.5}Ga_{1.5}O_{12}$ compound for the Rietveld analysis were collected at room temperature using a Bruker D8 ADVANCE powder diffractometer equipped with a VANTEC linear detector (CuKα radiation). The 2θ step size was 0.016° and the counting time was 2 s per step. These structures were taken as a starting model for the Rietveld refinement performed using the TOPAS 4.2 software. X-ray diffraction pattern of sample is presented in Fig. 1.

According to the X-ray diffraction data, the compound consists of

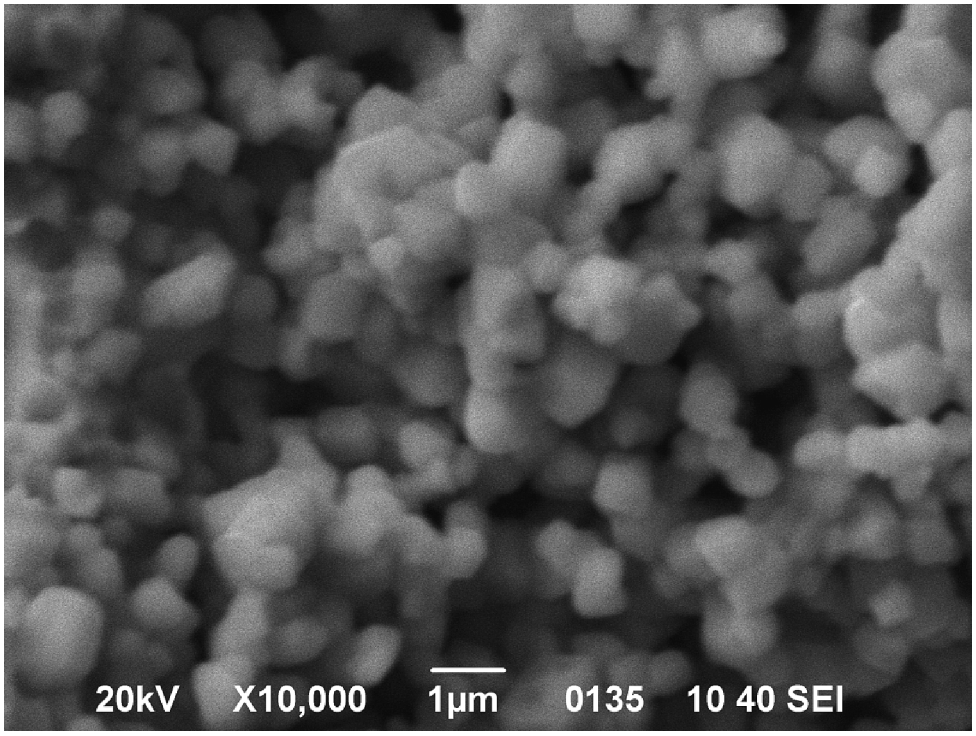

Fig. 2. SEM image of the $Y_{1.8}Bi_{1.2}Fe_{3.5}Ga_{1.5}O_{12}$ and $Bi_2Fe_4O_9$ compound.

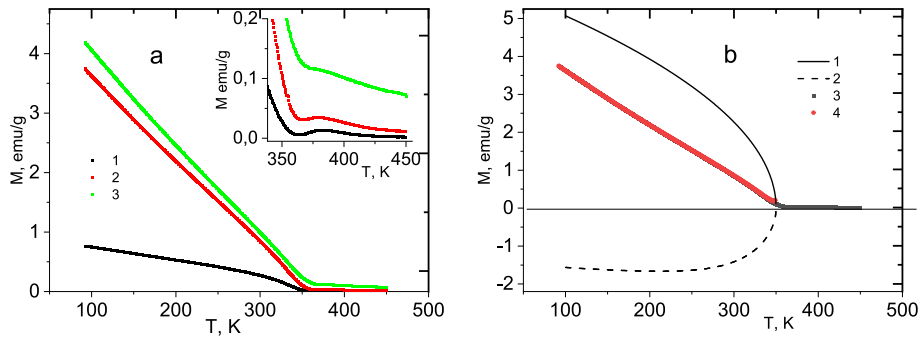

Fig 3. Magnetization of $Y_{1.8}Bi_{1.2}Fe_{3.5}Ga_{1.5}O_{12}$ and $Bi_2Fe_4O_9$ compound versus temperature in magnetic fields H = 100 Oe (1), 1 kOe (2), 10 kOe (3) (a). Sublattice magnetization calculated in model (4) with four-spin exchange A_1/J = 0.1 (1), A_2/J = 0.56 (2), resulting magnetization: experiment (3), theory (4). Insert: magnetization in the vicinity of the magnetic transition.

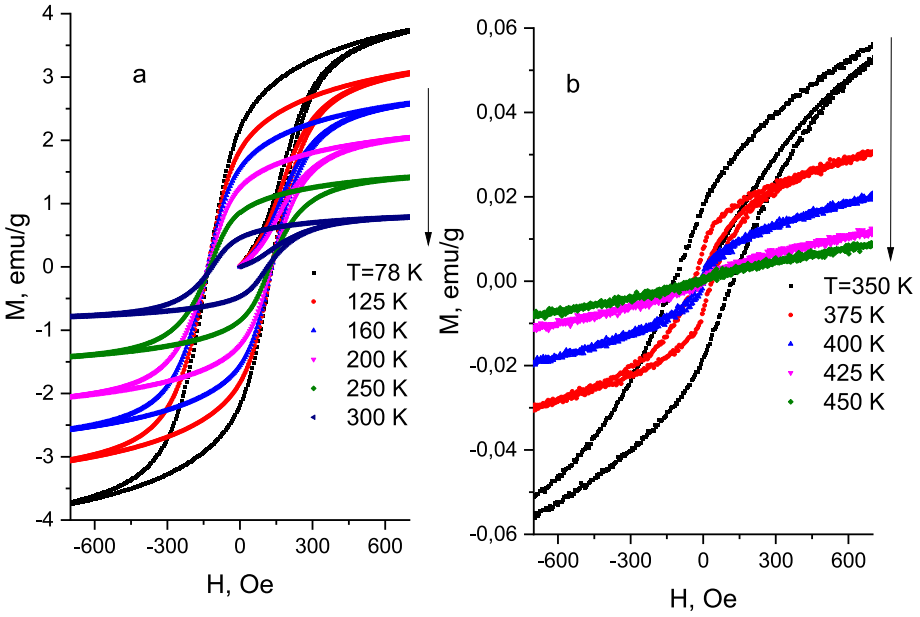

Fig. 4. The magnetization of $Y_{1.8}Bi_{1.2}Fe_{3.5}Ga_{1.5}O_{12}$ from the magnetic field at T = 78 K, 125 K, 160 K, 200 K, 250 K, 300 K (a), T = 350 K, 375 K, 400 K, 425 K, 450 top down (b).

$Bi_2Fe_4O_9$ (6.19%) and (YBi)3(FeGa)5O12 (93.81%) (Fig. 1). Bismuth-Substituted Diluted Yttrium Iron Garnet $Y_{1.8}Bi_{1.2}Fe_{3.5}Ga_{1.5}O_{12}$ corresponds to the space group Ia-3d and $Bi_2Fe_4O_9$ to the orthorhombic structure *Pbam* [26]. Parameters of elementary cells are given in Table 1.

The microstructure and morphology of the system were investigated by high-resolution scanning electron microscopy (SEM) on a Hitachi TM3000 microscope (Japan). The surface morphology study of the $Y_{1.8}Bi_{1.2}Fe_{3.5}Ga_{1.5}O_{12}$ and $Bi_2Fe_4O_9$ compound yielded an average grain size of ~ 400 nm (Fig. 2).

The magnetic measurements were performed on a LakeShore VSM 8604 vibrating sample magnetometer at the Center for Collective Use of the Krasnoyarsk Scientific Center, Siberian Branch of the Russian Academy of Sciences. A spherical sample with a mass of $m = 11.9$ mg and a diameter of $d = 1.48$ mm was placed in a continuous-flow cryostat of a LakeShore VSM 8604 facility. The temperature dependences of the magnetization in a field of $H = 1$ kOe were measured upon heating after cooling in different modes: zero-field cooling (zfc) and cooling in a field of 12 kOe (fc 12 kOe). The temperature range was from 78 to 450 K. The IR spectra were recorded on an FSM 2202 IR Fourier spectrometer with a spectral resolution of 0.5 cm^{-1} in the temperature range of 80–500 K and a wavenumber range of 450–7000 cm^{-1} with an average over 100 measurements. The spin of iron ions and their distribution over octahedra and tetrahedra were determined from the Mössbaur spectra on an MS-1104Em spectrometer with a Co^{57}(Rh) source on powder absorbers with a thickness of 5 mg/cm^2.

3. Magnetic measurements

Diluted bismuth ferrite is a ferrimagnet. Iron ions are replaced by gallium ions mainly in tetrahedral sites. Fig. 3 shows the dependences of the saturation magnetization and magnetization in the fields weaker than the coercive field. The partial replacement of yttrium by bismuth ions leads to the linear temperature dependence qualitatively different from the classical YIG behavior: $M = M_0(1 - T/T_C)^{0.5}$ at $T > 0.6T_C$ [27]. In polycrystalline $Y_3Fe_{3.5}Ga_{1.5}O_{12}$ containing one percent of Fe^{2+}, the $M(T)$ curve above 100 K is satisfactorily described by a power law [7].

Above room temperature, the magnetization exhibits the anomalous behavior, the $M(T)$ curve has minima at $T = 360$ K ($H = 100$ Oe) and 364 K ($H = 1000$ Oe) and, upon heating, passes through maxima at $T = 382$ K ($H = 100$ Oe) and 380 K ($H = 1000$ Oe) (see the inset in Fig. 3). In

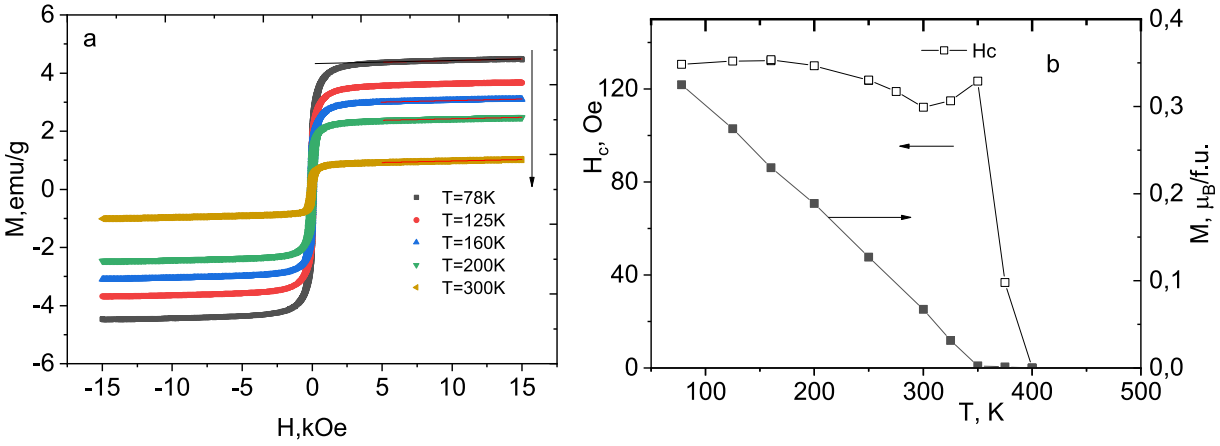

Fig. 5. Magnetization of $Y_{1.8}Bi_{1.2}Fe_{3.5}Ga_{1.5}O_{12}$ from a magnetic field at T = 78 K, 125 K, 160 K, 200 K, 300 K (a). Remanent magnetization (right axis) and coercive field Hc (left axis) versus temperature (b).

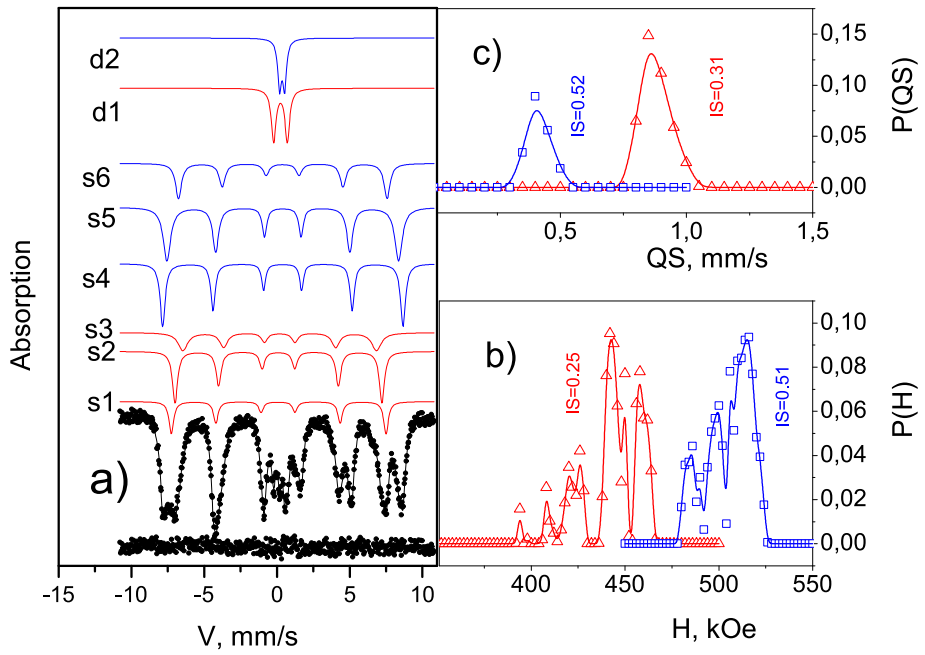

Fig.6. A) Mössbauer spectra of garnet at 78 K. Colored lines show components of the spectrum, the parameters of which are given in Table 2. Below the spectrum the error spectrum is shown - the difference between the experimental and calculated spectra. b) – Probability distribution of hyperfine fields in the experimental spectrum. c) - Probability distribution of quadrupole splittings in the experimental spectrum.

strong fields, the maximum turns into a step. The dM/dT derivatives have two extrema in the ranges of 337–334 and 394–395 K. Mullite $Bi_2Fe_4O_9$ has antiferromagnetic structure. Neel temperature depend on a synthesis method and a crystallite size. The $Bi_2Fe_4O_9$ samples obtained by the solid-state synthesis have a Néel temperature of $T_N = 258$ K [28] and $T_N = 238$ K in the single-crystal state [29]. Magnetization of polycrystalline bismuth ferrite $Bi_2Fe_4O_9$ undera 1 T field grows at heating from 0.13 emu/g at 4 K to 0.14 emu/g at room temperature [30]. The contribution of mullite to the magnetization of diluted bismuth ferrite will be 0.5% and will be absent in remanent magnetization.

The magnetization versus magnetic field curve exhibits a hysteresis (Fig. 4), which disappears at 400 K because the compound passes into the paramagnetic state (Fig. 4b). The remanent magnetization decreases linearly up to 350 K, has a kink at this temperature, and vanishes at 400 K (Fig. 5b). The coercivity varies within 10% up to 350 K and drops sharply upon further heating (Fig. 5b). The coercive field (Hc) is determined by the ratio of the anisotropy constant (K), the grain size (d) to the thickness of the domain wall (δ). For garnet ferrites, $Hc \sim Kd/(\mu_0 Ms\ \delta)$ reaches a maximum when $d = \delta$ coincides, when the grain size reaches 80 nm [31]. As the grain size increases $d > \delta$, the coercive field is determined by domain wall pinning at grain defects, segregation at grain boundaries, internal stresses, and dislocations. The weak dependence of the coercive force on temperature indicates that the functional temperature dependences of the anisotropy field and the exchange field are similar.

The saturation magnetization of the $Y_{1.8}Bi_{1.2}Fe_{3.5}Ga_{1.5}O_{12}$ compound differs from the values for conventional ferromagnets; in particular, the magnetization change ΔM at 0.2–1 T decreases by 10% from $\Delta M = 0.116$ to 0.103 emu/g upon heating from 80 to 250 K (Fig. 5a).

The YIG magnetization per formula unit is 4.55 μ_B/f.u. If gallium is only located in the tetrahedral sublattice, then, at the 50% replacement of iron ions in the tetrahedron by nonmagnetic atoms, the magnetization of the *a* sublattice will halve and the resulting magnetization will be $M = 2.1\mu_B$/f.u. The experimental asymptotic saturation magnetization of $Y_{1.8}Bi_{1.2}Fe_{3.5}Ga_{1.5}O_{12}$ at $T = 0$ is.

$$M = Ms \times \mu/5585 = 0.66\ \mu_B/\text{f.u.}, \quad (1)$$

where M_s is the saturation magnetization (emu/g) and μ is the molar weight of the compound. The experimental value is three times less than the theoretical one, which suggests the replacement of iron ions in octahedral sites. The coercivity of YIG is about 6 Oe and changes insignificantly upon gallium substitution [32,33]. The anisotropy constant decreases almost linearly with temperature, which is explained in the model $K_a \sim M^2 = (1 - T/T_C)$ [34]. The substitution of bismuth ions enhances the coercivity in $Y_{1.8}Bi_{1.2}Fe_{3.5}Ga_{1.5}O_{12}$. In the 90-nm-thick $Bi_{2.8}Y_{0.2}Fe_5O_{12}$ films, the room-temperature coercivity is 200 Oe [35,36]. The distribution of iron cations and their valence will be determined from the Mössbauer spectra.

4. Mossbauer effect and IR vibrational mode

The Mössbauer spectrum at 78 K is shown in Fig. 6a. We assume that the spectrum consists of two sextets (one with a chemical shift of<0.3 mm/s (tetrahedra) and the other with a chemical shift of>0.3 mm/s (octahedra)) and two doublets with the similar condition. The Mössbauer spectrum was interpreted in two stages. At the first stage, the distributions of hyperfine magnetic fields $P(H)$ and quadrupole splittings $P(QS)$ in the experimental spectrum were determined for two different isomer shifts. The chemical shifts common for each group of sextets and doublets and the amplitudes of the spectrum components were adjusted. The $P(H)$ and $P(QS)$ peaks and features indicate possible nonequivalent iron sites. At the second stage, based on these distributions, a model spectrum was built and then fitted to the experimental spectrum by varying all the hyperfine parameters.

According to the density functional theory (DFT) calculation, the isomer shift increases with the iron ion coordination number [37] and metal–ligand bond length; shorter bonds cause decreasing isomer shifts [38]. Three tetrahedral and three octahedral sites can be distinguished in the spectra. The peak in a local field of 407 kOe is within one percent, which is less than the measurement error and can be ignored. The strong substitution of gallium for iron at $\times = 1$ leads to the formation of three octahedral and two tetrahedral sites with weight ratios of $A_{oc} = 39\%$ and $A_{tet} = 61\%$ [12]. The formation of three octahedra and two tetrahedra was observed in $Er_3Fe_{4.2}Ga_{0.8}O_{12}$ [39] and upon substitution of aluminum in $Y_3Al_xFe_{5-x}O_{12}$ [40,41]. Gallium ions are distributed mainly

Table 2
Mössbauer parameters of garnet at 78 K. IS is the isomer chemical shift relative to α-Fe, *H* is the hyperfine field on the iron core, QS is the quadrupole splitting, $W_{34\text{-}16}$ is the width of the inner 34 and outer 16 sextet lines, and *A* is the area under the partial component of the spectrum (population of a nonequivalent site).

	IS, MM/c ± 0.01	H, кЭ ± 5	QS, MM/c ± 0.02	$W_{34\text{-}16}$, MM/c ± 0.02	A, % ± 4	Position
s1	0.20	458	0.05	0.38	17	Fe^{3+}(A)
s2	0.21	443	0	0.41	19	
s3	0.30	419	0	0.49–0.79	11	
s4	0.59	515	0.01	0.32–0.41	27	Fe^{3+}(d)
s5	0.51	498	0	0.37–0.61	8	
s6	0.50	483	0.02	0.49	7	
d1	0.31	0	0.94	0.38	7	Fe^{3+}(A)
d2	0.52	0	0.34	0.31	3	Fe^{3+}(d)

over tetrahedral sites (56% and 10%) and over octahedral sites (20%, 8%, and 6%). The spread of local fields is caused by a random distribution of gallium ions over the sublattices. The significant growth of the isomer shift in a weak local exchange field was attributed to a higher Ga concentration around the corresponding octahedral site.

The resolution of the spectrum components under the assumption that the Mössbauer effect probabilities for nonequivalent iron sites are identical allows us to establish the cationic distribution. The Mössbauer parameters of $Y_{1.8}Bi_{1.2}Fe_{3.5}Ga_{1.5}O_{12}$ are given in Table 2. It can be seen that 55% of iron contained in the sample occupies tetrahedral *a* sites and 45% of iron, octahedral *d* sites. Iron ions in mullite $Bi_2Fe_4O_9$ are equally distributed over octahedrons and tetrahedra with in a weight ratio of three percent, which can be ignored at estimation of distributing iron ions in garnet [42]. Using the Mössbauer spectroscopy data, we can estimate the magnetization. In the formula, there are 3.5 magnetic iron atoms in total; 48% of them are in the *a* sites with a sublattice magnetization of $Ma = 1.68gS_a$ and 42% are in the *d* sites with $M_d = 1.47gS_d$. The resulting magnetization is $M = 0.21gS_a = 1.05\ \mu_B$/f. u., where $S_{a,\ b}$ are the effective moments of the sublattices under the condition that the *g* factor is $g = 2$. The magnetization was estimated under the assumption of the antiparallel sublattice magnetic moments. In some studies, the discrepancy between the magnetization determined from the Mössbauer spectra and the magnetic measurement data is explained by a noncollinear structure caused by the enhancement of the exchange field inside the sublattice over the intersublattice exchange [12]. The decreasing magnetization is possibly due to the spin contraction at the site and formation of a noncollinear spin structure.

Substitution of bismuth for yttrium in $Y_{3-x}Bi_xFe_5O_{12}$ does not disturb the ratio between iron ions in octahedral and tetrahedral sites in a concentration range of x = 0–0.5 [43]. The isomer shifts are ~0.35 and 0.2 mm/s for octahedral and tetrahedral sites, respectively. As the Bi concentration increases from 0 to 0.5, the magnetic hyperfine field increases for both octahedral and tetrahedral sites from 483 and 391 kOe to 491 and 397 kOe and the quadrupole splitting also increases from 0.05 to 0.08 mm/s and 0.01 mm/s, respectively. This growth of the magnetic hyperfine fields reflects the enhancement of the superexchange near the diamagnetic substitution, but the saturation magnetization decreases linearly by 10% [43]. Possibly, the bismuth substitution up to 1.2 will reduce the magnetization by 20%.

The effect of the 6% mullite phase on the distribution of gallium ions over tetrahedral and octahedral sites in Table 2 is studied using Mössbaur and IR spectroscopy. The Mössbaur spectrum of the $Bi_2Fe_4O_9$/$BiFeO_3$ composite with a percentage ratio of 67/33 was measured continuously for three days (data set). Bismuth, like lead, absorbs gamma radiation, so the intensity of gamma quanta in mullite drops sharply and the sensitivity of the MS-1104Em spectrometer does not allow determining the spectrum from iron atoms at 78 K. The concentration of bismuth ions in mullite $Bi_2Fe_4O_9$ per formula unit is 15%, in $Y_{1.8}Bi_{1.2}Fe_{3.5}Ga_{1.5}O_{12}$ about 6%. Therefore, the Mössbauer spectrum measured on the MS-1104Em setup is determined only by iron atoms in $Y_{1.8}Bi_{1.2}Fe_{3.5}Ga_{1.5}O_{12}$.

The spectra of the $Y_{1.8}Bi_{1.2}Fe_{3.5}Ga_{1.5}O_{12}$ compound include two pairs of doublets with a high isomer shift and quadrupole splitting caused by the electric field gradient. The value of the quadrupole interaction depends on the electric field gradient induced on a nucleus by the electron cloud and neighboring ions [44]. The fully or half-filled e_g and t_{2g} orbitals do not contribute to the quadrupole splitting and the main contribution for the Fe^{3+} ion is related to the lattice. During the HS–LS transition, the $2T_{2g}$ term with one unpaired electron at the t_{2g} level is formed in the octahedron and the QS contribution changes from lattice to electron. By means of the lone electron pair, bismuth ions change the Bi–O bond length, distort the octahedron and tetrahedron, weaken the crystal field, and lead to the growth of admixing of the T_{1g} state to the ground state A_{1g}. Strengthening of the spin–phonon interaction in the octahedra (tetrahedra) surrounded by two bismuth ions can result in a local paramagnetic state of Fe^{3+} ions, which lacks a part of the exchange couplings. The second mechanism may be associated with the transition of the Fe^{3+} ion to the LS state. Depending on the mechanism, there are two options of the distribution of paramagnetic ions over octahedra and tetrahedra. In the case of the spin–phonon mechanism, paramagnetic ions are localized in octahedra and tetrahedra. In the LS state, iron ions are in the octahedron, because the energy of the HS–LS transition in the tetrahedron is several times higher. The mechanism of finding iron ions in the LS state contradicts the Mösbauer data. The divalent state of Fe^{2+}

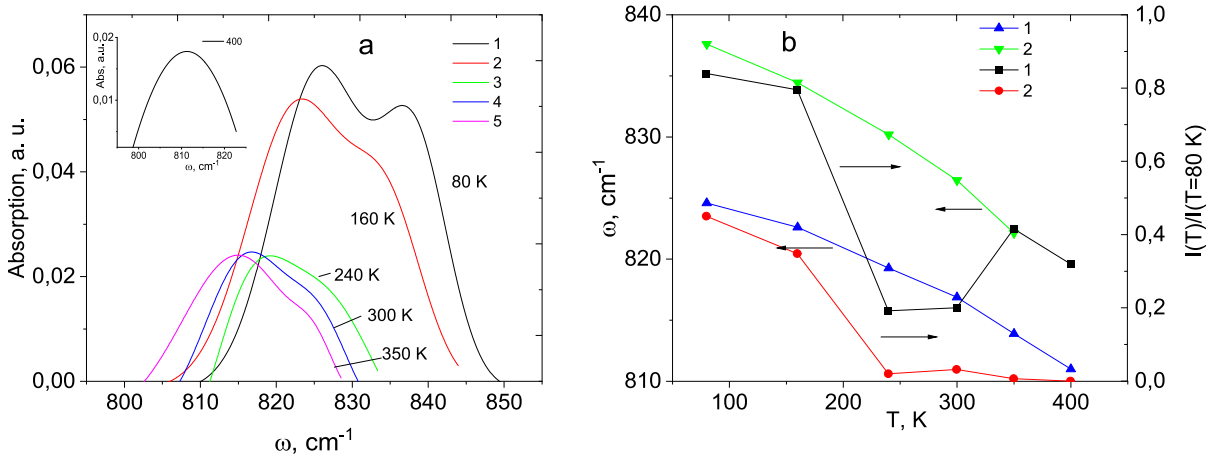

Fig. 7. IR absorption in $Y_{1.8}Bi_{1.2}Fe_{3.5}Ga_{1.5}O_{12}$ at temperatures of 80 K (1), 160 K (2), 240 K (3), 300 K (4), 350 K (5), 400 K (inset) (a), absorption frequencies поглощения ω_1 (1) и ω_2 (2) and their intensities I(T)/I(T = 80 K) (1), (2) versus temperature (b).

iron ions was not found in the Mössbaur spectra. In this case, the isomeric shift is greater than IS > 1 mm/s.

In the IR spectrum of the $Y_{1.8}Bi_{1.2}Fe_{3.5}Ga_{1.5}O_{12}$ compound, the absorption in the range of 800–850 cm^{-1} was found (Fig. 7a). The absorption spectrum is fitted by the two modes with the frequencies and intensities decreasing upon heating (Fig. 7b). Above 200 K, the intensity decreases several times and, at 350 K, one of the modes disappears, while the intensity of the other mode passes through a maximum. Upon heating from 80 to 350 K, the frequency decreases by 2%. The presence of this mode can be related to bismuth ions. The vibrational mode with $\omega = 820$ cm^{-1} was observed for several pyrochlore-structure compounds, for example, $Bi_3/2Zn_{0.92}Nb_{1.5}O_{6.92}$ and $Bi_3/2MgNb_3/2O_7$ [45], as well as for the $Bi_2(Sn_{1-x}Fe_x)_2O_7$ bismuth stannates [46]. The IR spectra of these compounds were interpreted by the difference between the Bi–O' bond lengths in the Bi2O' sublattice. The shift of the O' anion and Bi cation within a domain leads to the shortening of one Bi–O' bond and elongation of the other [47,48]. It was noted that the Bi and O' ions shift in all pyrochlores due to the 6 s^2 hybridization of an active lone electron pair with the cation *d* orbitals in Bi, which leads to the difference between the bond lengths [49]. The change in the Bi–O bond length in the $Y_{1.8}Bi_{1.2}Fe_{3.5}Ga_{1.5}O_{12}$ compound changes the Fe–O–Fe indirect exchange interaction. The T_{2g} mode is caused by the rotation of octahedra in the *XY* and *ZX* planes [50]. The rotation of octahedra at 240 K will change the intensity of the modes. The mechanism of the electron–phonon interaction in $Y_{1.8}Bi_{1.2}Fe_{3.5}Ga_{1.5}O_{12}$ is confirmed by a decrease in the intensity of the phonon mode in the $Bi_2(Sn_{0.7}Fe_{0.3})_2O_7$ IR spectrum by a factor of 2 at 260 K. The normalized *g* factor (*g*-2) changes its sign at 240 K, which is attributed to the deformation of the octahedron and the nonlinearity of elastic properties [51]. In YIG, the optical magnon mode at a frequency of 805 cm^{-1} is close to the phonon mode [52], which allows the energy redistribution between the magnetic and elastic subsystem.

The presence of gallium ions in $Bi_2Fe_4O_9$ mullite can also be determined from IR spectra. The vibrational frequency of the tetrahedron associated with its stretching is determined by the bond length of the cation and anion. In $Bi_2Fe_4O_9$ mullite, the bond length in the Fe-O tetrahedron is 0.186 nm, and in the Fe-O octahedron it is 0.202 nm [53]. When substituting with gallium, the bond length in the tetrahedron decreases Ga-O = 0.175 nm in $Bi_2Ga_4O_9$. The frequency of Fe-O-Fe symmetrical stretching vibration for tetrahedral site coordination is $\omega = 814$ cm^{-1} and Ga-O-Ga is $\omega = 850$ cm^{-1} at the room temperature [54]. The vibration frequencies in our samples at T = 300 K are equal to w = 816 cm^{-1} and 826 cm^{-1}. The second mode is attributed to $A_{1g} + T_{2g}$ combination mode $Y_{1.8}Bi_{1.2}Fe_{3.5}Ga_{1.5}O_{12}$. The absence of the vibration frequency w = 850 cm^{-1} in mullite in our samples indicates that gallium is not included in the mullite lattice. Perhaps this is due to the technology of sample synthesis.

5. Model

Upon substitution of gadolinium ions, the Curie temperature of YIG decreases almost linearly with the increasing gadolinium concentration: 30% of gadolinium in the garnet will reduce the Curie temperature from 560 K to $T_C(x) = (1 - x) \bullet 560$ K = 392 K. The substitution of bismuth for yttrium will strengthen the magnetoelastic coupling by means of the electron density redistribution on the Bi–O bonds at the shift of oxygen ions. The strong interaction with the lattice can result in the four-spin exchange coupling $AS^4 \sim (\frac{dJ}{\vartheta D})^2$, where ϑ_D is the Debye temperature and *dJ* is the spin–lattice interaction constant. At the competition between the bilinear and four-spin exchanges, there is a critical *A*/*J* value for the spin S = 1/2 at which the long-range magnetic order vanishes [55]. The antiferromagnetic state in the 2D Heisenberg model with the anisotropy $1 - J_{x,y}/J_z = 0.1$ transforms into a quantum spin liquid with the power-law behavior of the spin–spin correlation functions at *A*/*J* = 0.8, according to the Monte Carlo calculations [56]. Upon heating, the spin correlator increases in the longitudinal components and attains its maximum at the temperature of the spin liquid–paraphase transition, while the transverse components the correlator decrease. In the classical Heisenberg model with the continuous spin in a simple cubic lattice, the antiferromagnetic state passes into a noncollinear ferrimagnet with a spontaneous magnetic moment at $A/J = 1$ and the sublattice canting angle is determined as $\cos(\vartheta) = J/AS^2$ [57,58].

Table 3
Local exchange fields H_{ex}^{d} in the octahedron and H_{ex}^{a} the tetrahedron, statistical weights W_i,

H_{ex}^{d}	6 J	5 J	4 J	3 J	2 J	J
Wi	0,14	0,4	0,3	0,22	0,03	0,004
H_A^{tet}	4 J	3 J	2 J	J		
Wi	0,22	0,48	0,24	0,06		

In the polycrystalline $Y_{1.8}Bi_{1.2}Fe_{3.5}Ga_{1.5}O_{12}$ compound, we assume the presence of a spin–lattice coupling, which, at certain interaction parameters, results in a noncollinear spin configuration [59,60]. To qualitatively interpret the linear temperature dependence of the magnetization, we assume the existence of the four-spin exchange in the octahedral and tetrahedral sublattices:

$$H = -\sum_{i,j} J_{ij} S_i S_j - \sum_{i,j,k,l} A_{ij,kl} \left(\vec{S}_i \cdot \vec{S}_j\right)\left(\vec{S}_k \cdot \vec{S}_l\right) \quad (2)$$

where $J_{ij} < 0$ is the exchange between iron spins in octahedra and tetrahedra and $A_{ij,kl} < 0$ is the four-spin exchange in the sublattices. The exchange interactions of spins in the sublattices are ignored, since they are weaker than $J_{dd}/I_{da} = 1/7$ and $J_{aa}/J_{da} = 0.09$ by an order of magnitude [52]. Next, we simplify the problem and consider the spin sublattice in the form of a square with the spins in strong exchange field H_{ex}:

$$H = -H_{ex}\sum_i S_i - A_{12,34}\left(\vec{S}_1 \cdot \vec{S}_2\right)\left(\vec{S}_3 \cdot \vec{S}_4\right) - A_{13,24}\left(\vec{S}_1 \cdot \vec{S}_3\right)\left(\vec{S}_2 \cdot \vec{S}_4\right) \quad (3)$$

where the spin is quasi-Ising: S = –1, 0, 1. The effective sublattice magnetization has the form:

$$M_{SUB} = \frac{e^{-\frac{2A}{T}} sh\frac{4H_{ex}}{T} + 2e^{\frac{2A}{T}} sh\frac{2H_{ex}}{T} + sh\frac{H_{ex}}{T} + 3sh\frac{2H_{ex}}{T} + 3sh\frac{3H_{ex}}{T}}{e^{-\frac{2A}{T}} ch\frac{4H_{ex}}{T} + 4e^{\frac{2A}{T}} ch\frac{2H_{ex}}{T} + 6 + 4ch\frac{H_{ex}}{T} + 4ch\frac{2H_{ex}}{T} + 4ch\frac{3H_{ex}}{T} + 6e^{-\frac{2A}{T}}} \quad (4)$$

Fig. 3b presents the sublattice magnetizations (Eq. (4) with parameters of *A*/*J* = 0.56 and 0.1. The resulting magnetization depends linearly on temperature and describes the experimental results. At 350 K, the nonlinear interaction between the modes caused by the electron–lattice coupling vanishes, which eliminates the four-spin interaction. As a result, the temperature of the magnetic phase transition in the system with the bilinear exchange increases.

Let us now consider the conditions for the formation of paramagnetic ions. The random statistical distribution of gadolinium ions over the lattice leads to the disappearance of the Fe–Gd exchange interactions. In the garnet-structure lattice with the random distribution of diamagnetic atoms, the exchange field distribution function is formed. Table 3 gives the local exchange fields H_{ex}^{d} in the octahedron and H_{ex}^{a} in the tetrahedron and statistical weights W_i.

According to the Mössbauer data, the concentration of paramagnetic ions in tetrahedra is approximately twice as high as in octahedra, which is consistent with a statistical weight of $W_d = 0.03$ for the local field $H_{ex}^{d} = 2J$ and $W_a = 0.06$ for $H_{ex}^{a} = J$. Paramagnetic doublets in Mossbauer spectra were observed in dilute bismuth ferrite $BiFe_{1-x}Cr_xO_3$ in the magnetically ordered region at $T \ll T_N$ [61].

The paramagnetic spins make a significant contribution to the saturation magnetization and explain a decrease in the differential saturation magnetic susceptibility $\chi_d = dM/dH$ ($H \gg H_c$) upon heating. A

Table 4
Relative changes ΔM_H obtained in the molecular field approximation ($n = 1/2$, $H = 10$ kOe) and in the experiment ($n = 1$). Saturation magnetization reductions ΔM_{ex} (experiment), ΔM_{th} (theory), and ΔM_{PM} (due to the paramagnetic contribution).

T, K	ΔM_{ex}, μ_B/f.u.	ΔM_{PM}, μ_B/f.u.	$\Delta M_H(n = 1/2)$ μ_B/f.u.	$\Delta M_H(n = 1)$ μ_B/f.u.	ΔM_{th}, μ_B/f.u.
80	0,019	0,013	0,0014	0,003	0,014–0,016
250	0,017	0,004	0,0035	0,007	0,008–0,011

Note: Table 2 repeated renumbered.

decrease in the magnetization ΔM by 12% upon heating from 80 to 250 K in fields of 0.1–1 T is dictated by the two competing factors: the growth of the spin fluctuations upon heating and the drop of the paramagnetic contribution $\Delta M_{PM} = wg^2\,\mu_B^2\,S(S+1)\,H/3kT$, where w is the concentration of paramagnetic Fe^{3+} ions. For a qualitative conception of the increase in differential saturation magnetic susceptibility upon heating, we use the temperature dependence of magnetization obtained in the mean field theory (Landau theory). The Curie temperature increases in a magnetic field, which leads to an increase in the saturation magnetization $M_H(T) = M_0(1 - T/(T_c + H))^n$ as compared with the case of zero magnetic field: $M(T) = M_0(1 - T/T_c)^n$. The relative changes $\Delta M_H(T) = H/(2(T_c - T))$ obtained in the mean field theory ($n = 1/2$, $H =$ 10 kOe) and in the experiment ($n = 1$) are given in Table 4.

The model explains qualitatively the experiment. To obtain the quantitative agreement, it is necessary to take into account the four-spin interaction, the contribution of which to the magnetization decreases upon heating (Table 4).

6. Conclusions

Using the Mössbauer study, the distribution of iron ions over octahedral and tetrahedral sites in polycrystalline garnet ferrite $Y_{1.8}Bi_{1.2}Fe_{3.5}Ga_{1.5}O_{12}$ was established. The paramagnetic states of the spins of iron ions were found, the contribution of which explains a decrease in the differential magnetic susceptibility in the saturation region upon heating. Two critical temperatures were determined: the first one corresponding to the linear disappearance of the magnetization is the temperature of the compensation of the sublattice magnetizations and the second one is the temperature of the disappearance of the magnetization hysteresis and spontaneous magnetic moment. The coercivity was found to be almost temperature-independent. A disappear of the combined $A_{1g} + T_{2g}$ mode in the region of the magnetic phase transition was observed. The magnetic properties were explained within the model of the competing bilinear and four-spin exchanges.

CRediT authorship contribution statement

S.S. Aplesnin: Writing – original draft. **F.V. Zelenov:** Investigation, Software, Visualization, Writing – review & editing. **S.V. Semenov:** . **O. A. Bayukov:** .

Declaration of Competing Interest

The authors declare that they have no known competing financial interests or personal relationships that could have appeared to influence the work reported in this paper.

Data availability

Data will be made available on request.

Acknowledgments

The investigation of powder diffraction, Mössbauer spectra and magnetic measurements were performed using equipment from the Center for Collective Use, Krasnoyarsk Scientific Center, Siberian Branch of the Russian Academy of Sciences. The authors are grateful to T. N. Tarasenko for providing samples for magnetic measurements.

References

[1] V. Cherepanov, I. Kolokolov, V. L'vov, The saga of YIG: Spectra, thermodynamics, interaction and relaxation of magnons in a complex magnet, Phys. Rep. 229 (81) (1993) 81–144.
[2] P. Pirro, T. Bracher, A. V. Chumak, B. Lagel, C. Dubs, O. Surzhenko, P. Gornert, B. Leven, B. Hillebrands, Spin-wave excitation and propagation in microstructured waveguides of yttrium iron garnet/Pt bilayers, Appl. Phys. Lett. 104 (2014) 012402. https://doi.org/10.1063/1.4861343.
[3] A.V. Chumak, V.I. Vasyuchka, A.A. Serga, B. Hillebrands, Magnon spintronics, Nature Phys. 11 (2015) 453–461, https://doi.org/10.1038/nphys3347.
[4] M. Levy, O.V. Borovkova, C. Sheidler, B. Blasiola, D. Karki, F. Jomard, M. A. Kozhaev, E. Popova, N. Keller, V.I. Belotelov, Faraday rotation in iron garnet films beyond elemental substitutions, Optica 6 (5) (2019) 642–646, https://doi.org/10.1364/OPTICA.6.000642.
[5] B.J.H. Stadler, T. Mizumoto, Integrated magneto-optical materials and isolators: a review, IEEE Photon. J. 6 (2014) 0600215.
[6] Š. Višňovský, V. Prosser, Temperature compensation point in yttrium gallium iron garnet, Phys. Status Solidi A 10 (1) (1972) K97–K99.
[7] P. Hansen, P. Röschmann, W. Tolksdorf, Saturation magnetization of gallium-substituted yttrium iron garnet, J. Appl. Phys. 45 (6) (1974) 2728–2732.
[8] I. Bsoul, R. Olayaan, Structural and Magnetic Properties of $Er_3Fe_{5-x}Ga_xO_{12}$ Garnet, Mater. Res. Express 6 (2019), 076114, https://doi.org/10.1088/2053.
[9] M. Gaponov, S. Ovcharenko, N. Ilyin, E. Mishina, Laser-Induced Magnetization Dynamics in Si-Doped Yttrium-Iron Garnet Film, Condens. Matter 7 (4) (2022) 55, https://doi.org/10.3390/condmat7040055.
[10] M. Deb, P. Molho, B. Barbara, Jean-Yves Bigot, Phys. Rev. B 97 (2018), 134419, https://doi.org/10.1103/PhysRevB.97.134419.
[11] M. Deb, Ultrafast optical control of magnetization dynamics in polycrystalline bismuth doped iron garnet thin films, Appl. Phys. Lett. 107 (2015) 252404, https://doi.org/10.1063/1.493853.
[12] K. Hamasha, Q.I. Mohaidat, M. Lataifeh, I. Bsoul, S.H. Mahmood, Structural and Magnetic Studies of Ga-doped Yttrium Iron Garnet, Journal of Wuhan University of Technology-Mater, Sci. Ed. 36 (1) (2021) 13–21, https://doi.org/10.1007/s11595-021-2372-3.
[13] A. Scaramucci, E. Bousquet, M. Fechner, M. Mostovoy, N.A. Spaldin, Linear Magnetoelectric Effect by Orbital Magnetism, Phys. Rev. Lett. 109 (19) (2012), 197203, https://doi.org/10.1103/PhysRevLett.109.197203.
[14] S.S. Aplesnin, A.N. Masiugin, M.N. Sitnikov, T, Ishibashi, Substrate Effect on the Magnetoelectric Effect of Rare Earth-Substituted Bismuth Garnet Ferrite Films, JETP Lett. 110 (3–4) (2019) 204–212, https://doi.org/10.1134/S0370274X19150128.
[15] S.S. Aplesnin, A.N. Masyugin, M.N. Volochaev, T. Ishibashi, Coexistence of the Electric Polarization and Conductive Current in the Bismuth-Neodymium Ferrite Garnet Films, J. Mat. Sci: Mater Electron 32 (3) (2021) 3766–3781, https://doi.org/10.1007/s10854-020-05121-9.
[16] A.I. Popov, D.I. Plokhov, A.K. Zvezdin, Symmetry and magnetoelectric effects in garnet crystals and films, Phys. Rev. B 90 (21) (2014), 214427, https://doi.org/10.1103/PhysRevB.90.214427.
[17] A.S. Logginov, G.A. Meshkov, V.A. Nikolaev, A.P. Pyatakov, A.K. Zvezdin, Magnetoelectric control of domain walls in a ferrite garnet film, JETP Lett. 86 (2) (2007) 15–118, https://doi.org/10.1134/S0021364007140093.
[18] A.P. Pyatakov, D.A. Sechin, A.S. Sergeev, A.V. Nikolaev, E.P. Nikolaeva, A. S. Logginov, A.K. Zvezdin, Magnetically switched electric polarity of domain walls in iron garnet films, EPL, IOP Publishing 93 (1) (2011) 17001.
[19] A.K. Zvezdin, A.P. Pyatakov, Inhomogeneous magnetoelectric interaction in multiferroics and related new physical effects, Phys.-Usp. 52 (8) (2009) 845–851.
[20] A. Raja, P.M.M. Gazzali, G. Chandrasekaran, Enhanced electrical and ferrimagnetic properties of bismuth substituted yttrium iron garnets, Phys. B: Condensed Matter 613 (2021) 412988.
[21] S. Geller, Z. Kristallogr, Crystal chemistry of the garnets, Cryst. Mater. 125 (1967) 1–47, https://doi.org/10.1524/zkri.1967.125.16.1.
[22] I. Lyubutin, S. Starchikov, I. Troyan, Y. Nikiforova, M. Lyubutina, A. Gavriliuk, Pressure Induced Spin Crossover and Magnetic Properties of Multiferroic $Ba_3NbFe_3Si_2O_{14}$, Molecules 25 (17) (2020) 3808.
[23] P. Gütlich, A.B. Gaspar, Y. Garcia, Spin state switching in iron coordination compounds, Beilstein J. Org. Chem. 9 (2013) 342–391, https://doi.org/10.3762/bjoc.9.39.
[24] M.M. Dîrtu, C. Neuhausen, A.D. Naik, A. Rotaru, L. Spinu, Y. Garcia, Insights into the Origin of Cooperative Effects in the Spin Transition of $[Fe(NH_2trz)_3](NO_3)_2$: the Role of Supramolecular Interactions Evidenced in the Crystal Structure of $[Cu(NH_2trz)_3](NO_3)_2{\cdot}H_2O$, Inorg. Chem. 49 (2010) 5723–5736, https://doi.org/10.1021/ic100667f.
[25] F.V. Zelenov, T.N. Tarasenko, O.E. Kovalev, Z.F. Kravchenko, V.V. Burkhovetskii, V.I. Mikhailov, A.V. Golovchan, Magnetostriction in ferrit-granite synthesized by modify method of combustion gel in ethyleenglycol, Izvestia RAN, Seriya Fizicheskaya 87 (3) (2023), https://doi.org/10.31857/S036767652270065X.
[26] M.K. Verma, V. Kumar, T. Das, R.K. Sonwani, V.S. Rai, D. Prajapati, K. Sahoo, V.K. Kushwaha, A. Gupta, K. Mandal, Synthesis of $Bi_2Fe_4O_9$ Crystalline Ceramic as

Extremely Capable Photocatalyst via Proficient Chemical Route, J. Miner. Mater Char Eng., 9 (2021) 444-461. https://DOI: 10.4236/jmmce.2021.95030.
[27] D.F. Strenzwilk, E.E. Anderson, Calculation of the Sublattice Magnetization of Yttrium Iron Garnet by the Oguchi Method, Phys. Rev. 175183 (1968) 654. Erratum Phys. Rev. 183 (1969) 608.
[28] A.A. Zatyupo, L.A. Bashkirov, I.O. Troyanchuk, G.S. Petrov, A.I. Galyas, L.S. Lobanovsky, S.V. Trukhanov, I.M. Sirota, Magnetization, magnetic susceptibility, effective magnetic moment of Fe^{3+} ions in ferit $Bi_2Fe_4O_9$, Inorg. Mat. 49 (2013) 658-662. https://Doi: 10.7868/S0002337X13060201.
[29] M.N. Iliev, A.P. Litvinchuk, V.G. Hadjiev, M.M. Gospodinov, V. Skumryev, E. Ressouche, Phonon and magnon scattering of antiferromagnetic $Bi_2Fe_4O_9$, Phys. Rev. B, 81 (2010) 024302(8). https://DOI: 10.1103/PhysRevB.81.024302.
[30] Z. Tian, S. Yuan, X. Wang, X. Zheng, S. Yin, C. Wang, L. Liu, Size effect on magnetic and ferroelectric properties in $Bi_2Fe_4O_9$ multiferroic ceramics, J. Appl. Phys. 106 (2009), 103912, https://doi.org/10.1063/1.3259392.
[31] P. Hansen, J.P. Krumme, D. Mergel, Garnets and ferrites for magneto-optical recording, J. Magn. Soc. Jpn. 15 (1991) 219–226.
[32] E. Garskaite, K. Gibson, A. Leleckaite, J. Glaser, D. Niznansky, A. Kareiva, On the synthesis and characterization of iron-containing garnets ($Y_3Fe_5O_{12}$, YIG and $Fe_3Al_5O_{12}$, IAG), Chem. Phys. 323 (2–3) (2006) 204–210.
[33] Noorhana Yahya, Goh Kah Hean, High Saturation Induction for Bi-Substituted Yttrium Iron Garnet Prepared Via Sol Gel Technique, Am. J. Appl. Sci. 4 (2) (2007) 80–84, https://doi.org/10.3844/ajassp.2007.80.84.
[34] D.T.T. Nguyet, Nguyen Phuc Duong, Temperature-dependent magnetic properties of yttrium iron garnet nanoparticles prepared by citrate sol–gel, J. Alloy. Compd. 541 (2012) 18–22, https://doi.org/10.1016/j.jallcom.2012.06.122.
[35] Q.I. Mohaidata, M. Lataifeha, K. Hamashab, S.H. Mahmood, I. Bsould, M. Awawdeha, The Structural and the Magnetic Properties of Aluminum Substituted Yttrium Iron Garnet, Mater. Res. 21 (3) (2018), https://doi.org/10.1590/1980-5373-MR-2017-0808.
[36] V. Berzhansky, T. Mikhailova, Magneto-optics of nanoscale Bi:YIG films, Appl. Opt. 52 (26) (2013) 6599, https://doi.org/10.1364/AO.52.006599.
[37] Menil, Systematic trends of the ^{57}Fe Mössbauer isomer shifts in (FeOn) and (FeFn) polyhedra. Evidence of a new correlation between the isomer shift and the inductive effect of the competing bond T-X (→ Fe) (where X is O or F and T any element with a formal positive charge), J. Phys. Chem. Solids 46 (1985) 763.
[38] F. Neese, Prediction and interpretation of the ^{57}Fe isomer shift in Mössbauer spectra by density functional theory, Inorg. Chim. Acta 337 (2002) 181, https://doi.org/10.1016/S0020-1693(02)01031-9.
[39] I. Bsoul, R. Olayaan, M. Lataifeh, Q.I. Mohaidat, S.H. Mahmood, Structural and magnetic properties of $Er_3Fe_{5-x}Ga_xO_{12}$ garnets, Mater. Res. Express 6 (7) (2019), 076114, https://doi.org/10.1088/2053-1591/ab198b.
[40] D. Rodic, M. Mitric, R. Tellgren, H. Rundlof, The cation distribution and magnetic structure of $Y_3Fe_{(5-x)}Al_xO_{12}$, J. Magn. Magn. Mater. 232 (1–2) (2001) 1–8, https://doi.org/10.1016/S0304-8853(01)00211-6.
[41] Q.I. Mohaidata, M. Lataifeha, K. Hamashab, S.H. Mahmoodc, I. Bsould, M. Awawdeha, The Structural and the Magnetic Properties of Aluminum Substituted Yttrium Iron Garnet, Mater. Res. 21 (3) (2018), https://doi.org/10.1590/1980-5373-MR-2017-0808.
[42] N. Shamir, E. Gurewitz, H. Shaked, The magnetic structure of $Bi_2Fe_4O_9$ – analysis of neutron diffraction measurements, Acta Crystallogr. A 34 (1978) 662–666.
[43] M. Niyaifar, M.C. Ramani, M. Radhakrishna, A. Mozaffari, J.A. Hasapour, Magnetic studies of BixY3-xFe5O12 fabricated using conventional method, Hyperfine Interact. 187 (1–3) (2008) 1223–1227, https://doi.org/10.1007/978-3-540-78697-9_168.
[44] N.N. Greenwood, T.C. Gibb, Mössbauer Spectroscopy, Chapman and Hall Ltd, 1971, p. 659.
[45] R.L. Withers, T.R. Welberry, A.-K. Larsson, Y. Liu, L. Noren, H. Rundlof, F.J. Brink, Local crystal chemistry, induced strain and short range order in the cubic pyrochlore (Bi1.5−αZn0.5−β) (Zn0.5−γNb1.5−δ)O(7–1.5α−β−γ−2.5δ) (BZN), J. Solid State Chem. 177 (2004) 231, https://doi.org/10.1016/j.jssc.2003.07.005.
[46] L.V. Udod, S.S. Aplesnin, M.N. Sitnikov, O.B. Romanova, M.N. Molokeev, Phase transitions in bismuth pyrostannate upon substitution of tin by iron ions, J. Alloy. Compd. 804 (2019) 281–287, https://doi.org/10.1016/j.jallcom.2019.07.020.
[47] R.A. McCauley, Infrared-absorption characteristics of the pyrochlore structure, J. Opt. Soc. Am. 63 (6) (1973) 721–725.
[48] M. Avdeev, M.K. Hass, J.D. Jorgensen, R.J. Cava, Static disorder from lone-pair electrons in $Bi_{2-x}M_xRu_2O_7$-y (M = Cu, Co; x=0,0.4) Pyrochlores, J. Solid State Chem. 169 (1) (2002) 24–34.
[49] A.L. Hector, S.B. Wiggin, Synthesis and Structural Study of Stoichiometric $Bi_2Ti_2O_7$ Pyrochlore, J. Solid State Chem. 177 (1) (2004) 139–145, https://doi.org/10.1016/S0022-4596(03)00378-5.
[50] M.N. Iliev, A.P. Litvinchuk, Phonon and magnon scattering of antiferromagnetic $Bi_2Fe_4O_9$, Phys. Rev. B 81 (2010), 024302, https://doi.org/10.1103/PhysRevB.81.024302.
[51] L. Udod, S. Aplesnin, M. Sitnikov, O. Romanova, O. Bayukov, A. Vorotinov, D. Velikanov, G. Patrin, Magnetodielectric effect and spin state of iron ions in iron-substituted bismuth pyrostannate, EPJP 135 (2020) 776, https://doi.org/10.1140/epjp/s13360-020-00781-2.
[52] A.J. Princep, R.A. Ewings, S. Ward, S. Tóth, C. Dubs, A.T. Boothroyd, The full magnon spectrum of yttrium iron garnet, npj Quantum Mater. 2 (63) (2017), https://doi.org/10.1038/s41535-017-0067-y.
[53] M. MangirMurshed, GwilhermNé nert , ManfredBurianek , LarsRobbena, ManfredM¨ uhlberg, Hartmut Schneider, ReinhardX.Fischer , ThorstenM.Gesing Temperature-dependentstructuralstudiesofmullite-typeBi2Fe4O9, J. Solid State Chem. 197 (2013) 370. dx.doi.org/10.1016/j.jssc.2012.08.062.
[54] A. Beran, E. Libowitzky, M. Burianek, M. Mühlberg, C. Pecharroman, H. Schneider, Infrared and raman spectroscopy of mullite-type $Bi_2Ga_4O_9$, Cryst. Res. Technol. 43 (2008) 1230, https://doi.org/10.1002/crat.200800396.
[55] S.S. Aplesnin, Quantum spin liquid in an antiferromagnet with four-spin interactions, Phys. Solid State 39 (8) (1997) 1246–1250.
[56] S.S. Aplesnin, N.I. Piskunova, Influence of the four-spin exchange interaction on the magnetic properties of manganites, J. Phys. Condens. Matter 17 (37) (2005) 5881, https://doi.org/10.1088/0953-8984/17/37/023.
[57] E.L. Nagaev, Magnetics with complex exchange interaction, Moskow, Science (1988.-) 231p.
[58] S.S. Aplesnin, Magnetic and electrical properties of strongly correlated magnetic semiconductors with four-spin interaction and orbital ordering. Moskow, Fizmatlit, 2013, -171 p.
[59] S.S. Aplesnin, Quantum Spin Liquid in an Antiferromagnetic Chain with Spin-Phonon Interaction with S = ½, Phys. Met. Metall. 96 (3) (2003) 264–270. https://doi.org/10.48550/arXiv.cond-mat/0207118.
[60] S.S. Aplesnin, Two-dimensional quantum spin liquid with S = 1/2 spins interacting with acoustic phonons, Phys. Lett. A 333 (5–6) (2004) 446–449, https://doi.org/10.1016/j.physleta.2004.10.064.
[61] I.P. Raevski, S.P. Kubrin, A.V. Pushkarev, N.M. Olekhnovich, Y.V. Radyush, V. V. Titov, M.A. Malitskaya, S.I. Raevskaya, H. Chen, The effect of Cr substitution for Fe on the structure and magnetic properties of BiFeO3 multiferroic, Ferroelectrics 525 (1) (2018), https://doi.org/10.1080/00150193.2018.1432844.